Shell Mix in the Compressed Core of Spherical Implosions

S. P. Regan, J. A. Delettrez, F. J. Marshall, J. M. Soures, V. A. Smalyuk, B. Yaakobi, R. Epstein, V. Yu. Glebov, P. A. Jaanimagi, D. D. Meyerhofer,* P. B. Radha, T. C. Sangster, W. Seka, S. Skupsky, C. Stoeckl, and R. P. J. Town
Laboratory for Laser Energetics, University of Rochester, 250 East River Road, Rochester, New York 14623-1299

D. A. Haynes, Jr. and I. E. Golovkin
Department of Engineering Physics, University of Wisconsin, Madison, Wisconsin 53706

C. F. Hooper, Jr.†
Department of Physics, University of Florida, Gainesville, Florida 32611

J. A. Frenje, C. K. Li, R. D. Petrasso, and F. H. Séguin
Plasma Science and Fusion Center, Massachusetts Institute of Technology, Cambridge, Massachusetts 02139
(Received 13 December 2001; published 2 August 2002)

The Rayleigh-Taylor instability in its highly nonlinear, turbulent stage causes atomic-scale mixing of the shell material with the fuel in the compressed core of inertial-confinement fusion targets. The density of shell material mixed into the outer core of direct-drive plastic-shell spherical-target implosions on the 60-beam, OMEGA laser system is estimated to be $3.4(\pm 1.2)$ g/cm^3 from time-resolved x-ray spectroscopy, charged-particle spectroscopy, and core x-ray images. The estimated fuel density, $3.6(\pm 1)$ g/cm^3, accounts for only ~50% of the neutron-burn-averaged electron density, $n_e = 2.2(\pm 0.4) \times 10^{24}$ cm^{-3}.

DOI: 10.1103/PhysRevLett.89.085003 PACS numbers: 52.70.La, 32.70.–n, 52.35.Py, 52.50.Jm

In the compressed core of laser-driven inertial-confinement fusion (ICF) targets, hot, dense plasmas are produced with electron densities and temperatures comparable to those of stellar interiors (i.e., $n_e \geq 10^{25}$ cm^{-3} and $T_e \geq 1$ keV) [1]. Spherical capsules containing fuel of hydrogen isotopes are directly irradiated by a large number of symmetrically arranged laser beams in the direct-drive approach to ICF [2]. Hydrodynamic instabilities typically cause ICF target performance including primary neutron yield, and compressed fuel and shell areal densities to fall short of 1D predictions [2]. As the shell accelerates, perturbations that result from laser-irradiation nonuniformities (i.e., laser imprint) and target imperfections are amplified by the Rayleigh-Taylor (RT) instability [3–6]. These front surface perturbations feed through the shell during their acceleration phase growth, seeding the deceleration-phase RT instability [7] on the inner surface. When the higher-density shell converges toward the target center and is decelerated by the lower-density fuel, the inner surface of the shell is subjected to the deceleration-phase RT instability. A central hot spot forms as the fuel is compressed, and its fusion rate peaks when the fuel temperature reaches its maximum value just before stagnation. In addition, the modulations grow due to Bell-Plesset convergent effects [8] throughout the implosion up to stagnation.

The unstable RT growth has been a subject of intensive experimental studies in planar [3–6], cylindrical [9], and spherical [10] geometries with both direct and indirect [11] (with x rays produced in a high-Z enclosure or hohlraum) drive. Recently, the growth of the deceleration-phase RT instability has been detected in a spherical implosion using shell radiography by the x rays coming from the hot core emitted near peak compression [12]. The classical RT instability of the deceleration-phase in its turbulent, highly nonlinear stage causes the shell material or pusher to mix on the atomic scale with the fuel. Fuel-pusher mix has the deleterious effects of diluting the fuel density and quenching the fuel temperature. The success of high-gain ICF target designs requires an understanding of the fuel-pusher mix in spherically imploding targets. This Letter describes the impact of hydrodynamic instabilities on spherical implosion target performance. It directly quantifies, for the first time, the amount of plastic-shell mixed into the outer core of compressed fuel capsules. It is of great importance to ICF because it provides a direct experimental observation of fuel-pusher mix that results in target performance degradation. In addition, it also shows for the first time using time-resolved x-ray spectroscopy, charged-particle spectroscopy, and core x-ray images that the deceleration-phase RT instability reaches the highly nonlinear, turbulent regime resulting in fuel-pusher mix on the atomic scale.

The density of shell material mixed into the outer core of direct-drive plastic-shell spherical-target implosions is estimated from a unique combination of time-resolved x-ray spectroscopic measurements, nuclear measurements of fuel areal density (ρR), and core x-ray images. The deuterium fuel within a plastic capsule is doped with trace amounts of Ar. The emissivity-averaged (i.e., averaged over the emitting volume and weighted to the emissivity) core electron density (n_e) and temperature (T_e) are determined by measuring the time-dependent, Stark-broadened, Ar K-shell emissions [13]. 1D hydrodynamics code simulations reveal that the emissivity-averaged spectroscopic

measurement probes the mantle of fuel surrounding the central hot spot (i.e., the mix region) [13]. The measured core n_e has contributions from the fuel, the Ar dopant, and the CH shell material that has mixed into the core [i.e., $n_e = n_e(\mathrm{D}) + n_e(\mathrm{Ar}) + n_e(\mathrm{CH})$]. Nuclear measurements of fuel ρR are combined with x-ray core images to estimate the fuel density. The estimated fuel density does not account for the measured core n_e averaged over the neutron temporal burn width; therefore, plastic-shell material that has mixed into the core must contribute the remaining electrons. Because these diagnostic spectral line shapes are only sensitive to the electron density within approximately a Debye length of the Ar radiator (i.e., $\sim$ a few Angstroms in these hot, dense plasmas), the shell material must mix with the Ar-doped fuel on the atomic scale.

This novel diagnostic technique provides a direct measurement of CH density in the compressed core of direct-drive implosions resulting from fuel-pusher mix. The results are consistent with a highly constrained model that inferred the core conditions and microscopic-scale fuel-shell mix based on nuclear diagnostics [2,14] and with previously reported spectroscopic indications of mix using targets with a thin embedded layer of solid Ti [15]. Other studies of fuel-pusher mix used simulations from a hydrodynamics code to interpret the measured time histories of x-ray spectroscopic signals from tracer layers in the fuel and pusher; however, they did not directly estimate the density of pusher material that is mixed into the core [16].

Time-resolved Ar K-shell spectroscopy has been established as a reliable technique to diagnose the compressed cores of direct-drive implosions [17] and indirect (x-ray)-drive implosions [18]. Two properties of the Ar K-shell spectrum emitted from hot, dense plasmas are exploited to infer a unique combination of emissivity-averaged core T_e and n_e: (i) The optically thin line shapes used herein depend strongly on density and are relatively insensitive to variations in T_e. (ii) The relative intensities of the Ar K-shell lines and their associated L-shell satellites are sensitive to variations in T_e and n_e [13].

High-density, direct-drive spherical implosions [2] were performed on the 60-beam, 30-kJ UV OMEGA laser system [19]. The three types of plastic capsules under consideration are shown in Fig. 1(a) with a 20-μm shell thickness, a 0.5-mm radius, and a 15-atm gas fill. The choice of gas fill was selected to optimize either the x-ray spectroscopy measurements or nuclear measurements of fuel ρR. The targets were driven with a 23-kJ, 1-ns square laser pulse smoothed with phase plates [20], 1-THz 2D smoothing by spectral dispersion (SSD) [21], and polarization smoothing (PS) using birefringent wedges [22]. The beam-to-beam rms power imbalance was 5% or less. Figure 1(b) shows a diagram of the pusher, the mix region, and the central hot spot of the compressed target at the time of peak neutron production. These implosions have predicted convergence ratios at stagnation of $\sim$15.

The fuel density is obtained from the DT capsule and the emissivity-averaged core n_e is obtained from the DD capsule with the Ar dopant. The Ar dopant has a limited effect on target performance. It reduces the primary neutron yield to $\sim$75% of an undoped target [2]. Dopant levels of Ar were minimized to reduce the impact of the enhanced radiative losses on target performance. The total fill pressure was 15 atm with an atomic Ar *percentage* of 0.18, resulting in a partial pressure of Ar of $\sim$0.05 atm. The measured ratio of secondary neutron production (Y_{2n}) to primary neutron production (Y_n) in the Ar-doped capsule $Y_{2n}/Y_n = 1.8 \times 10^{-3}$ is within the range observed for DD-only filled capsule implosions [23,24]. This shows that the compressed fuel areal density is not significantly affected by the Ar dopant. DD- and DT-gas-filled capsules in Fig. 1 were shown to have similar target performance [2]. For DT-filled implosions, the fuel ρR was determined to be $15(\pm 3)$ mg/cm^2 from the number of elastically scattered knock-on fuel particles: $n + D \rightarrow n' + D'$. This diagnostic of fuel ρR is insensitive to the core T_e profile [25,26]. Since the Ar-doped capsule has a similar performance to the DD-only capsule, and the 1D hydrodynamics code LILAC [27] predicts the DD-gas filled capsule will achieve about the same fuel density at peak neutron production as the DT capsule with a slightly larger convergence ratio; the fuel density inferred from the knock-on measurement of fuel ρR was taken to be representative of the Ar-doped implosions.

An average fuel density of $3.6(\pm 1)$ g/cm^3 is obtained by dividing the fuel $\rho R = 15(\pm 3)$ mg/cm^2 by the core radius $R = 42(+4)$-μm. The radius of the imploding core at the time of peak neutron production is estimated by

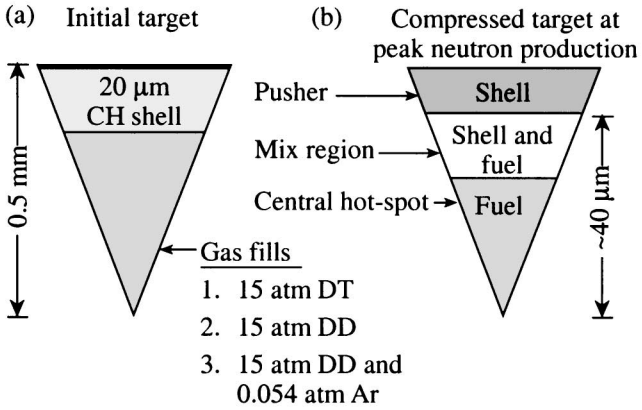

FIG. 1. (a) The initial plastic capsule with a 20-μm shell thickness, a 0.5-mm radius, and a 15-atm gas fill. The choice of gas fill was selected to optimize either the x-ray spectroscopy measurements or nuclear measurements of fuel ρR. (b) The pusher, the mix region, and the central hot spot (not drawn to scale) of the compressed target at the time of peak neutron production. Time-resolved Ar K-shell spectroscopy probes n_e and T_e of the mantle of fuel surrounding central hot spot (i.e., the mix region).

comparing the fuel mass $M_f = 1.09$-μg with the measured fuel $\rho R = 15(\pm 3)$ mg/cm^2 [i.e., $M_f = 4\pi R^2(\rho R)/3$]. The radius was also estimated to be $R = 38(\pm 5)$-μm from a high magnification ($25\times$), gated (~ 40 ps) pinhole camera image of ~ 4.5 keV x-ray emission from a DD-only filled capsule implosion that was recorded at the time of peak neutron production [13]. The core radius measured with the x-ray diagnostic is consistent with that estimated from the nuclear measurements. Using the fuel density estimated from the DT implosions, the contribution to the n_e from the fuel in the Ar-doped capsule is estimated to be $n_e(\mathrm{D}) = 1.1(\pm 0.3) \times 10^{24}$ cm^{-3}.

The emissivity-averaged core T_e and n_e were inferred from the measured time-dependent Ar K-shell spectral line shapes of the Ar He-β ($1s3l - 1s^2$), He-γ ($1s4l - s^2$), He-δ ($1s5l - 1s^2$), and Ly-β ($3l - 1s$) resonant transitions and associated satellites [13]. A flat crystal spectrometer outfitted with a streak camera recorded the spectra with a 25-ps temporal resolution [13]. The Stark-broadened line profiles for the Ar He-β, He-γ, He-δ, and Ly-β resonant transitions and associated satellites were calculated with the multi-electron radiator line shape (MERL) code [28] in the manner described in Ref. [29]. MERL utilizes the adjustable parameter exponential approximation [30] for ion microfield calculation, the theory of Boercker *et al.* [31] for the ion dynamics, and a quantum mechanical relaxation approximation for electron broadening [29]. Collisional-radiative-equilibrium population distributions are solved using the CRETIN code [32]. The effects of the radiative transfer of the optically thick Ly-α ($2l - 1s$) and He-α ($ls2l - 1s^2$) emissions on the populations are approximated using Mancini's escape factors [33]. Opacity broadening is calculated assuming uniform core conditions. The optical depths τ_0 of the diagnostic lines Ar He$_\beta$, Ar He$_\gamma$, and Ar Ly$_\beta$ are estimated to be less than one in this experiment.

The spectrum recorded at the time of peak T_e ($t = 1.93$ ns) is shown in Fig. 2, along with the modeled spectrum, which includes the contribution from the background x-ray continuum emission. The inferred T_e and n_e are $2.0(\pm 0.2)$ keV and $2.5(\pm 0.5) \times 10^{24}$ cm^{-3}. The best fit to the measured spectrum in the 3.5- to 4.0-keV range is determined using a least squares fitting routine. The time history of emissivity-averaged core T_e (triangles) and n_e (squares) inferred from the time-resolved, Ar K-shell spectroscopy is shown in Fig. 3. The measured x-ray continuum in the 3.50- to 3.55-keV range (solid line) is also shown. The T_e peaks first while the n_e peaks around the time of peak x-ray production. At peak compression (after peak neutron production) n_e increases to $3.1\ (\pm 0.6) \times 10^{24}$ cm^{-3} and T_e decreases to 1.7 ($\pm$ 0.17) keV. The falling T_e is caused by heat conduction to the shell and radiative losses. The T_e inferred from fitting the background x-ray continuum emission in the 3.5- to 4.0-keV spectral range slowly decreases with time from ~ 0.8 keV at $t = 1.77$ ns to ~ 0.5 keV at 2.15 ns. These inferred values are much lower than the T_e inferred from the Ar K-shell spectrum, which probes the fuel region. Therefore, it appears that most of the background emission in the spatially averaged measurement is from the colder and more massive shell. The accuracy in n_e is estimated to be $\pm 20\%$ and in T_e is estimated to be $\pm 10\%$ [13].

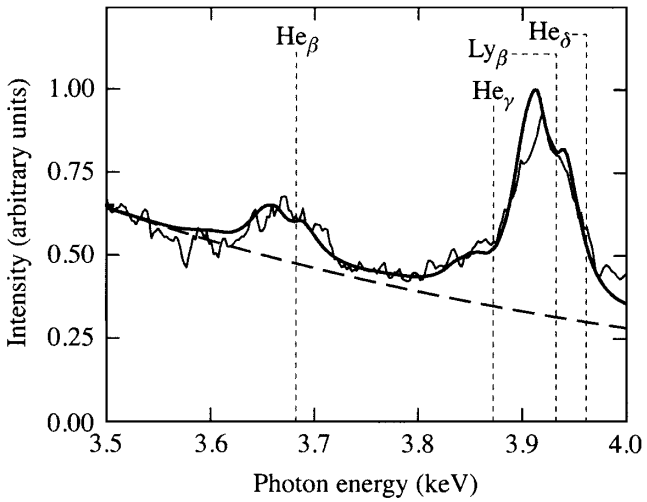

FIG. 2. The measured spectrum (thin curve) observed at $t = 1.93$ ns (estimated time of peak neutron emission) and the modeled spectrum (thick curve) in the 3.5- to 4.0-keV range are presented. The black dashed curve represents the background x-ray continuum emission spectrum and the vertical dotted lines represent the unshifted line centers of the Ar K-shell resonance lines. The inferred T_e and n_e are $2.0(\pm 0.2)$ keV and $2.5(\pm 0.5) \times 10^{24}$ cm^{-3}.

The relative timing of neutron-burn history with the n_e measurement must be established to compare the fuel ρR with the n_e measurement, since the time-integrated fuel areal density measurements are weighted to the time of

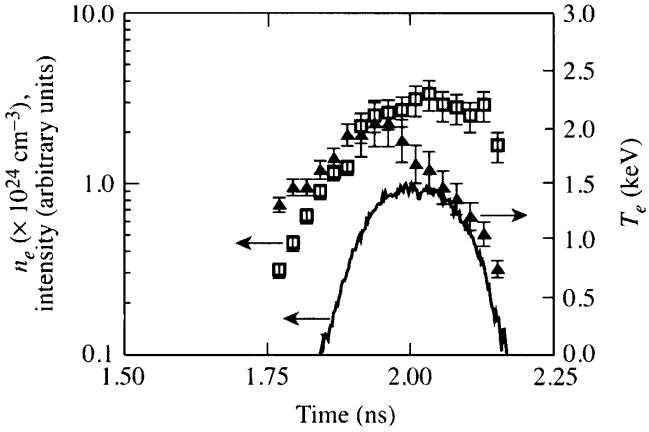

FIG. 3. The time history of the emissivity-averaged core T_e (triangles) and n_e (squares) inferred from the time-resolved Ar K-shell spectroscopy for shot number 22 507 reveals the T_e peaks first, followed by the n_e peaking around the time the x-ray continuum in the 3.50- to 3.55-keV range (solid line) peaks.

peak neutron emission. The measured neutron-burn history [2] shows that the peak neutron burn occurs $\sim$170 ($\pm$100) ps before the peak x-ray emission. To pinpoint the time of peak neutron emission within the experimental uncertainty of the timing, the predictions of a 1D hydrodynamics code are used. LILAC simulations of the implosion indicate that the peak neutron production occurs at the same time as the peak emissivity-averaged T_e. Therefore, the peak neutron production is assumed to be simultaneous with the peaking of the T_e at $t = 1.93$ ns.

In the mix region the emissivity-averaged n_e and T_e, averaged over the 170-ps FWHM neutron-burn width, are $n_e = 2.2(\pm 0.4) \times 10^{24}$ cm^{-3} and $T_e = 1.9(\pm 0.2)$ keV. The emissivity-averaged T_e is lower than the neutron-burn-averaged ion temperature $T_i = 3.7(\pm 0.5)$ keV measured with the neutron-time-of-flight detector, which is weighted to the peak ion temperature in the central hot spot. These observations are consistent with the centrally peaked electron and ion temperature profiles predicted by the 1D hydrodynamics code.

The estimated contribution to the n_e from the fuel accounts for only $\sim$50% of the measured core n_e that is averaged over the neutron-burn width. The contribution from the Ar dopant known from target metrology is 1.5% of the n_e. The remaining electrons [i.e., n_e (CH) = $1.1(\pm 0.4) \times 10^{24}$ cm^{-3}] must therefore come from the plastic-shell material that has mixed into the core, resulting in an estimated CH core density in the mix region of $3.4(\pm 1.2)$ g/cm^3. The estimated amount of CH mass in the mix region corresponds to $\sim$0.4-μm thickness of the initial 20-μm shell thickness. The inferred total pressure (i.e., electron + ion) in the mix region around the time of peak neutron production is $\sim$11 Gbar.

In conclusion, the Rayleigh-Taylor instability in its highly nonlinear, turbulent stage causes atomic mix of the shell material or pusher with the fuel in the compressed core of inertial-confinement fusion targets. The density of shell material mixed into the outer core has been estimated for the first time from a unique combination of time-resolved x-ray spectroscopic measurements, nuclear measurements of fuel areal density, and core x-ray images. The compressed cores of moderate-convergence-ratio (CR $\sim$ 15) direct-drive spherical implosions of plastic shells with a deuterium fill have been shown to have an estimated mass composition in the mantle of fuel surrounding the central hot spot of $\sim 1/2$ deuterium and $\sim 1/2$ CH, corresponding to a fuel density of $3.6(\pm 1)$ g/cm^3 and a CH density of $3.4(\pm 1.2)$ g/cm^3.

This work was supported by the U.S. Department of Energy Office of Inertial Confinement Fusion under Cooperative Agreement No. DE-FC03-92SF19460, the University of Rochester, and the New York State Energy Research and Development Authority. The support of DOE does not constitute an endorsement by DOE of the views expressed in this paper.

*Also at Departments of Mechanical Engineering, and Physics and Astronomy.
†Deceased.

[1] R. W. Lee, R. Petrasso, and R. W. Falcone, University of California Report No. UCRL119170, Lawrence Livermore National Laboratory, 1995.
[2] D. D. Meyerhofer *et al.*, Phys. Plasmas **8**, 2251 (2001).
[3] V. A. Smalyuk *et al.*, Phys. Rev. Lett. **81**, 5342 (1998).
[4] C. J. Pawley *et al.*, Phys. Plasmas **6**, 565 (1999).
[5] S. G. Glendinning *et al.*, Phys. Rev. Lett. **78**, 3318 (1997).
[6] G. Dimonte, Phys. Plasmas **6**, 2009 (1999).
[7] M. M. Marinak *et al.*, Phys. Plasmas **3**, 2070 (1996).
[8] M. S. Plesset, J. Appl. Phys. **25**, 96 (1954).
[9] W. W. Hsing *et al.*, Phys. Plasmas **4**, 1832 (1997).
[10] S. G. Glendinning *et al.*, Phys. Plasmas **7**, 2033 (2000).
[11] J. D. Lindl, Phys. Plasmas **2**, 3933 (1995).
[12] V. A. Smalyuk *et al.*, Phys. Rev. Lett. **87**, 155002 (2001).
[13] S. P. Regan *et al.*, Phys. Plasmas **9**, 1357 (2002).
[14] P. B. Radha *et al.*, Phys. Plasmas **9**, 2208 (2002).
[15] B. Yaakobi *et al.*, Phys. Plasmas **4**, 3021 (1997).
[16] T. R. Dittrich *et al.*, Phys. Rev. Lett. **73**, 2324 (1994).
[17] B. Yaakobi *et al.*, Phys. Rev. Lett. **44**, 1072 (1980).
[18] B. A. Hammel *et al.*, Phys. Rev. Lett. **70**, 1263 (1993).
[19] T. R. Boehly *et al.*, Opt. Commun. **133**, 495 (1997).
[20] Y. Lin, T. J. Kessler, and G. N. Lawrence, Opt. Lett. **21**, 1703 (1996).
[21] S. P. Regan *et al.*, J. Opt. Soc. Am. B **17**, 1483 (2000).
[22] T. R. Boehly *et al.*, J. Appl. Phys. **85**, 3444 (1999).
[23] F. H. Seguin *et al.*, Phys. Plasmas **9**, 2725 (2002).
[24] H. Azechi *et al.*, Laser Part. Beams **9**, 119 (1991).
[25] S. Skupsky and S. Kacenjar, J. Appl. Phys. **52**, 2608 (1981).
[26] C. K. Li *et al.*, Phys. Plasmas **8**, 4902 (2001).
[27] M. C. Richardson *et al.*, in *Laser Interaction and Related Plasma Phenomena*, edited by H. Hora and G. H. Miley (Plenum, New York, 1986), Vol. 7, p. 421.
[28] R. C. Mancini *et al.*, Comput. Phys. Commun. **63**, 314 (1991).
[29] D. A. Haynes, Jr., *et al.*, Phys. Rev. E **53**, 1042 (1996).
[30] C. A. Iglesias, J. L. Lebowitz, and D. A. MacGowan, Phys. Rev. A **28**, 1667 (1983).
[31] D. B. Boercker, C. A. Iglesias, and J. W. Dufty, Phys. Rev. A **36**, 2254 (1987).
[32] H. A. Scott and R. W. Mayle, Appl. Phys. B **58**, 35 (1994).
[33] R. C. Mancini, R. F. Joyce, and C. F. Hooper, Jr., J. Phys. B **20**, 2975 (1987).